J. Astrophys. Astr. (2002) **23,** 197–212

Spectral Measurements of Cyg X-3: A Thermal Source Embedded in Hot Plasma within a Cold Shell

R. K. Manchanda *Tata Institute of Fundamental Research, Homi Bhabha Road, Colaba, Mumbai 400 005, India.*
e-mail: ravi@tifr.res.in

Received 2002 August 23; accepted 2002 October 21

Abstract. The attempts at unified model fitting to explain the spectral variations in Cyg X-3 suggest equally probable fits with a combination of an absorbed blackbody and a separately absorbed power law with an exponential cut-off or a composite of absorbed free-free emission with a power law hard X-ray component apart from the iron emission line. These seemingly ordinary but ad hoc mixtures of simple X-ray emission mechanisms have a profound implication about the geometry of the X-ray source. While the first set suggests a black-hole nature of the compact object, the second combination is consistent with a neutron star binary picture. The spectral variability at hard X-ray energies above 30 keV can provide crucial input for the unified picture. In this paper, we present spectral observations of Cyg X-3, made in our on-going survey of galactic and extragalactic X-ray sources in the 20–200 keV energy region, using Large Area Scintillation counter Experiment. The data show a clear power-law photon spectrum of the form $\frac{\mathrm{d}N}{\mathrm{d}E} \sim E^{-2.8}$ in the 20 to 130 keV energy range. A comparison with earlier data suggests that the total number of X-ray photons in the entire 2–500 keV energy band is conserved at all time for a given luminosity level irrespective of the state. We propose that this behaviour can be explained by a simple geometry in which a thermal X-ray source is embedded in a hot plasma formed by winds from the accretion disk within a cold shell. The high/soft and low/hard X-ray states of the source are simply the manifestation of the extent of the surrounding scattering medium in which the seed photons are Comptonized and hot plasma can be maintained by either the X-ray driven winds or the magneto-centrifugal winds.

Key words. Low mass X-ray binaries—X-ray sources—Cyg X-3.

1. Introduction

Cyg X-3 is not only the most luminous binary system but can be classified as a class unto itself. The emission spectrum of the source extends from radio, infrared, X-ray to GeV gamma ray energies. In the X-ray energy band source exhibits both a 'high' state and a 'low' state with X-ray luminosity of the source varying between 2 and 10×10^{37} ergs s^{-1} for a source distance of 8.5 kpc. A hard X-ray spectrum, a 4.8^{h} period with an asymmetric light curve and quasi-periodic oscillations with a period of

few hindered seconds are the key temporal characteristics of the source. The quasi-periodic oscillations seen in the Cyg X-3 have the highest power at periods between 50 and 1500 sec and this is in complete contrast with the observations of other QPO sources where the excess power in the power density spectrum lies in the 1–50 Hz (van der Klis & Jenson 1985; Kitamoto *et al.* 1992). Despite a large number of data obtained since 1968, and the observations of a variety of temporal and spectral features from the source, the true nature of the source geometry and the X-ray emission mechanism still remains unresolved (see review by Bonnet-Bidaud & Chardin 1988; White *et al.* 1992).

In the X-ray band, the main spectral characteristics of the source include a black-body/power law spectrum at low energies attenuated by a large hydrogen column density, a simple power law spectrum above 20 keV (Rao *et al.* 1991; Chitnis *et al.* 1993; Dal Fiume *et al.* 2000) and an emission line feature at 6.5 keV arising from the iron line, which is more predominant during the low/hard state (Kitamoto *et al.* 1994a). The presence of an X-ray halo up to $\sim 2^\circ$ was seen in the Ginga data (Kafuko *et al.* 1994) and recent measurement of the halo with Chandra observatory (Predehl *et al.* 2000) reveal that surface brightness profile in the 5–7 keV and 1–3 keV band extends to a radial distance of 3° and 6° respectively. These data clearly point to the very large amount of surrounding material, which can also lead to build up effects due to multiple Compton scattering. The high resolution spectroscopy in the 1–10 keV using Chandra observatory shows a rich discrete emission line spectrum, which also implies an origin in the photo-ionization driven excitation of the surrounding medium (Paerels *et al.* 2000).

Cyg X-3 is not visible in the optical and UV band, probably due to its position in the galactic plane, but is clearly seen in the infrared band above 1 μm and shows clear 4.8^h binary modulation. Near simultaneous measurements in the IR and X-ray band with UKRIT and OSSE data show a fair degree of similarity in the binary light curve, thereby suggesting generic relations between the two (van Kerkwijk 1993; Matz *et al.* 1996). The source is also bright at the millimeter and centimeter wavelength and on occasions exhibits giant radio flares accompanied with relativistic outflow with velocity 0.3 c (Newell *et al.* 1998). At higher gamma ray energies there is no credible detection of the flux between 35 and 1000 MeV (Mori *et al.* 1997). Positive detection of sources in the TeV and PeV energy bands have been reported on several occasions, however, data were never confirmed in subsequent searches. Similarly, claims have been presented for the detection of 12.59 msec pulsation from the source at energies above $E > 100$ TeV however, no pulsation was observed in later attempts (Chadwick *et al.* 1985; Bhat *et al.* 1988; Chardin & Gerbier 1989; Rannot *et al.* 1994).

The 4.8^h period of the non-eclipsing light curve is typical of the low mass X-ray binaries. The observations of the Doppler shift in the He and N lines in the infrared spectrum of the companion suggest that the primary component is a Wolf Rayet star (van Kerkwijk *et al.* 1992, 1996). If the proposed association of Cyg X-3 with the Wolf-Rayet star is true, then Cyg X-3 is the shortest period binary among the known High Mass Binary Systems. A phase-on system geometry of the binary is inferred from the absence of 4.8^h modulation in the radio jets (Ogley *et al.* 2001). The true nature of the compact object in Cyg X-3 is however still unresolved. The system is generally believed to be a neutron star even though possibility of a black hole candidate has been discussed in literature (Schmutz *et al.* 1996; Ergam & Yungelson 1998).

2. Payload and the observations

The balloon-borne payload consists of an X-ray telescope made up of three modules of scintillation detectors having both passive and active shielding and fitted on a fully steerable alt-azimuth mount. Each of the detector modules has a geometrical area of 400 cm^2 and the thickness of the prime detector is 4 mm. Since the sensitivity limit in a scintillation counter mainly arises from the detector background generated by Compton scattering of high energy photons, the detector modules are a specially designed combination of thin and thick large area NaI(Tl) scintillation counters arranged in back to back geometry (Manchanda 1998). The 3σ sensitivity of the LASE telescope in the entire energy range up to 200 keV is $\sim 1 \times 10^{-6}\,cm^{-2}s^{-1}keV^{-1}$ for a source observation of 10^4 sec. The response matrix of each detector is constructed from the pre flight calibration of the detectors at different X-ray line energies using a variety of radioactive sources Am^{241}, Ba^{133}, Cd^{109}. To calibrate the high energy end of chosen energy range, we used highly accurate 'divide by two' attenuators in the detector outputs and observed the 300 keV and 357 keV lines from Ba^{133}. The field of view of each module is $4.5^o \times 4.5^o$ and is defined by demountable mechanical slat collimator specially designed with a sandwiched material of Lead, Tin and Copper effective up to 250 keV. Each module along with its collimator is further encased with a passive shield. Each detector is designed as a stand-alone unit with independent on-board subsystems for HV power and data processing. LASE payload is fully automatic with an on-board star tracker and requires no ground control during the flight. The details of the detector design, associated electronics, control subsystems and in-flight behaviour of instrument is presented elsewhere (D'Silva *et al.* 1998).

The balloon flight was launched on 30th March 1997 from Hyderabad, India (cut-off rigidity 16.8 GV) and reached a ceiling altitude of 3.3 mbs. Two detector modules were used for source observations during this flight. A number of X-ray sources Her X-1, GR 1744-28, GS 1843 + 00, GRS 1905 + 105, Cyg X-1 and Cyg X-3 were observed during the experiment. Cyg X-3 was in the field of view of the two detectors for a total period of 50 minutes during 0430 to 0530 UT. The background was derived from two observations of a blank field before and after the source pointing. The present observation of the source corresponds to MJD 50536.2 and corresponds to the binary phase of $\phi \sim 0.7376$ using the ephemeris of T_o = JD 2440 949.896 ± .0009 and $P_0 = .19968354 \pm 1.5 \times 10^{-7}$ d.

3. Results and discussion

A total excess of 30,000 photons due to Cyg X-3 was obtained in the two detectors during the entire observations and corresponds to a combined statistical significance of 60σ in the 20–165 keV energy band. The source contribution was divided in 12 energy bins and corrected for the atmospheric absorption of 3.3 mbs. corresponding to the altitude, window transmission, detection efficiency and the energy resolution of each detector. An additional correction of 10% due to the systematic effects was applied to data below 26 keV. The combined deconvolved hard X-ray spectrum of the source is shown in Fig. 1. It is seen from that, that the entire data can be fitted to a single power law of the form $\frac{dN}{dE} = K E^{-\alpha}$ ph $cm^{-2}s^{-1}keV^{-1}$. The best fit model parameters for a single power law are; $K = 16.3 \pm 1.6$ and $\alpha = -2.74 \pm 0.13$ for $\chi^2 \sim 0.17$ per degree

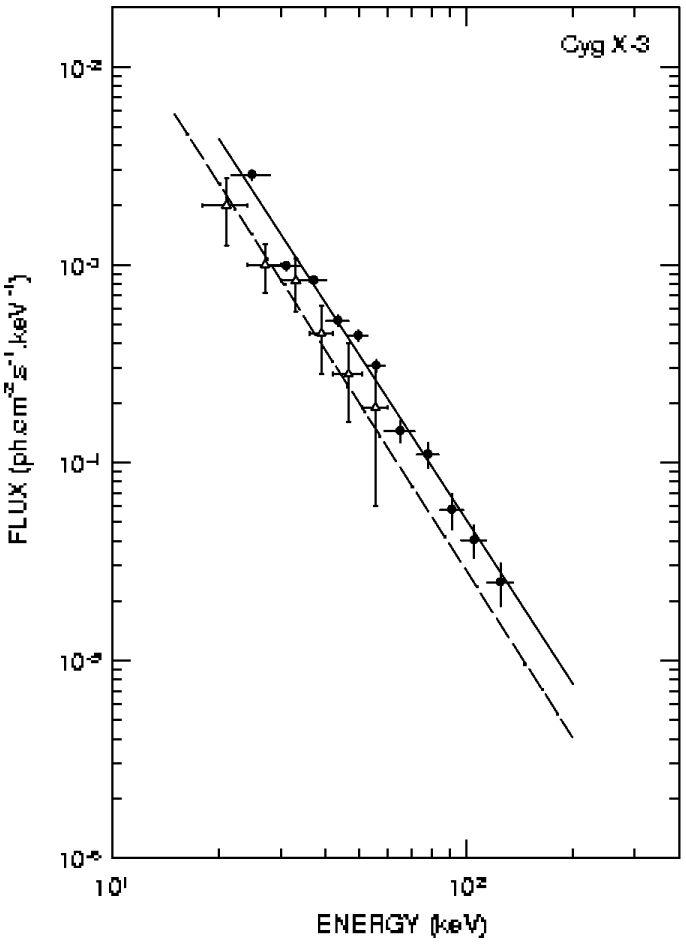

Figure 1. Hard X-ray spectra of Cyg X-3. Solid line represents the best fit to the data. The data of Rao *et al.* (1991) is shown for comparison (Δ).

of freedom. In Fig. 1, we have also plotted the phase averaged spectral data points of Cyg X-3 obtained by Rao *et al.* (1991) using a xenon filled proportional counter telescope for comparison and their best fit spectral shape $11.3\,E^{-2.8}$ (dotted line). It is clear from the figure that two data sets are in complete agreement in spectral shape and with a small change in magnitude representing the activity level of the source on the corresponding epoch. The estimated luminosity of the source in 20–200 band corresponding to our observations is 2×10^{37} ergs/sec, assuming a source distance of 10 kpc.

The arrival time of each accepted event, from any of the detector modules in the LASE payload is time-tagged with an accuracy of 25 μsec relative to the telemetry frame sync using UT time reference. For the analysis of timing properties of the Cyg X-3, we computed the arrival time of each photon and searched for the coherent pulsed emission at 12.6 msec once reported from the UHE data using XRONOS folding routine. Search was made between 11 and 13 msec using 100 steps. The data from two detectors were analyzed independently and co-added. No statistical

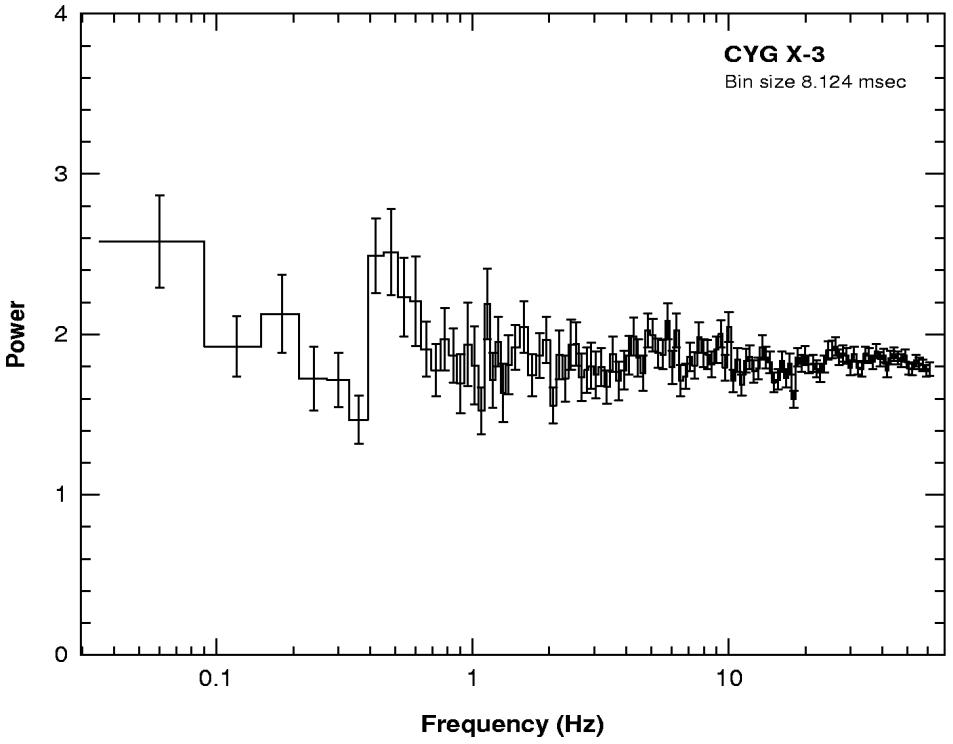

Figure 2. Power density spectrum using FTOOLS.

significant peak was found around the pulsar period of 12.57 msec. Similarly to search for the 121 sec transient period, we binned the data in 1 sec intervals and used the folding routine. Once again no clear single peak with large residual power was seen in the data. To look for the high frequency Quasi-periodic oscillations in our data, we rebinned the data with 8.1 msec resolution and reanalyzed the observed photons using FTOOLS. The power density spectrum is shown in Fig. 2. It is clear from the figure that there is no evidence of any dominant frequency in our data, however, a feature at 0.5 Hz is indicted but its significance is limited due to low statistics.

To determine the activity level of Cyg X-3 corresponding to the spectral and temporal data presented above, we have plotted X-ray light curves of the source taken from the archival data in Fig. 3. The top panel in Fig. 3 shows the X-ray light curve of the source from BATSE data on board CGRO in the 20–120 keV band. The all sky monitor data on-board RXTE in the 2–6 keV band is shown in the bottom panel. The expanded view in each panel is shown in the inset. The arrow in the figures indicates the epoch of the present observation of the source. It is seen from the figure that in the hard X-ray region, Cyg X-3 was close to its normal quiescent phase during the present observations. In the soft X-ray band however, the X-ray emission appears close to a flare like behaviour.

A simple power-law nature of the hard X-ray emission during the quiescent state as seen in Fig. 1, suggests a non-thermal origin for the X-ray photons. The hard X-ray emission in Cyg X-3 is believed to originate in the Inverse Compton scattering process of the low energy photons (Sunyaev & Titarchuk 1980; Liang & Nolan

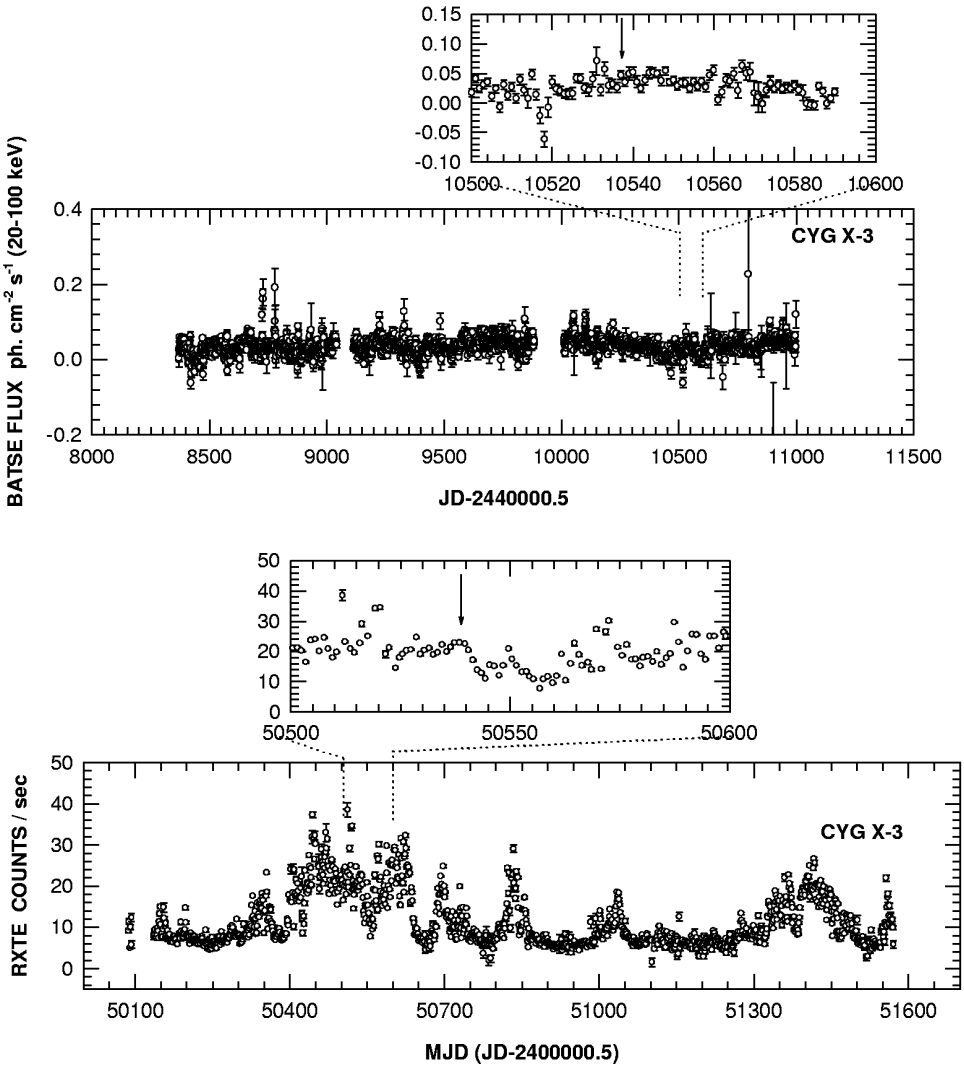

Figure 3. X-ray light curve of Cyg X-3 as seen in BATSE (upper panel) and RXTE data. The arrow indicates the epoch of the present observation.

1984). Comptonization of the low energy photons can provide a natural mechanism for the emission of high energy photons. During Comptonization the seed photons are upgraded in energy and the increase in photon energy on average during each scattering is given by $\frac{\nu'}{\nu} \sim 1 + \frac{4}{3}[\gamma^2 - 1]$. Therefore, multiple scattering even by a Maxwellian electron gas can lead to very high photon energies. But the final spectral shape will be determined by the energy spectrum of the electrons and the seed photons. In such a scenario, the spectral characteristics of the source should differ substantially during the active phase compared with the present observations. In figure 4 we have plotted the hard X-ray spectrum of the source during the flare state seen in OSSE data (Matz *et al.* 1994) and the high state data from HEXE (Maisack *et al.* 1994). The OSSE data correspond to the high state viewing period 7 during August 8–15, 1991 (MJD 48476)

just after the major radio flare. The HEXE data corresponds to the observations in May 1988. The dotted line in the figure gives the combined fit to both the data sets. It is seen from the figure that during the flare mode the hard X-ray spectrum of the source continues to be a power law but does have a much steeper spectrum with a spectral index 3.25 ± 0.15.

3.1 *Model geometry*

To arrive at a unified model of the source it is essential that all the observed features of the sources be put in proper perspective. The first attempt in this direction was made by White & Holt (1982) who modeled the observed HEAO-A2 data with a multi-parameter fit arising out of different emission mechanisms. A different set of parameters was obtained by Nakamura *et al.* (1993) while fitting the Ginga data in the 2–30 keV. Rajeev *et al.* (1994) tried to fit a similar model using EXOSAT data along with high energy measurements in the 20–60 keV band (Rao *et al.* 1991). In these models, a one-to-one comparison of the observed spectra has been carried out for data collected at different epochs. The complexity of the model can be judged from the summary of the derived parameters in these models, in which ad hoc emission/absorption features are introduced to improve the χ^2 value of the fit to the data. A functional fit to the observed high energy X-ray spectral data in the extended energy region up to 200 keV is not possible with the derived parameters of these models.

It is also clearly seen from the light curves presented in Fig. 3, that integral luminosity of the source does vary continuously and it is either uncorrelated or at best anti-correlated between the soft and hard X-ray bands. In addition, the source also exhibits asymmetric 4.8^h binary light curve. Therefore, any attempt to construct a unified model by a detailed comparison between different observations not made simultaneously can lead to art-effects. Even the simultaneous observations with different detectors in the broad energy band are prone to systematic effects. For example, the best fitted iron line energy from Ginga data is 6.53 ± 0.03 (Kitamoto *et al.* 1994a) and does not change with the intensity state. For the EXOSAT data the best fit iron line energy peak during high state is 6.95 ± 0.03 (Willingale *et al.* 1985). Similarly, in the case of Ginga data, the estimated value of N_H is the $3 \times 10^{22}\,\mathrm{cm}^{-2}$ and is the same during high and low states, while the derived numbers for EXOSAT data are not only higher by a factor ~ 1.5 but also vary by a factor of 3 between two states of the source (Nakamura *et al.* 1993). The absolute values of different parameters during a multi parameter fit is also a sensitive function of the number of parameters and their weightage factor. Therefore, only global properties can be used to delineate X-ray emission mechanism and the source geometry. In Fig. 5, we have plotted the observed spectral data in the 2–500 keV energy range. The low energy data corresponding to 2–30 keV band is taken from the Ginga observations of Nakamura *et al.* (1993). The data points correspond to both high and low states of the source. The most surprising feature of Fig. 5 is that the spectral index in the hard X-ray region as inferred earlier for the two luminosity states of the source appears to be a natural extension of the low energy data. A careful observation of the data shown in the figure suggests that the integral number of X-ray photons in the entire energy band of 2–500 keV are conserved during the two intensity states for a given activity level of the source. This conclusion leads to very fundamental changes in our understanding of the source geometry.

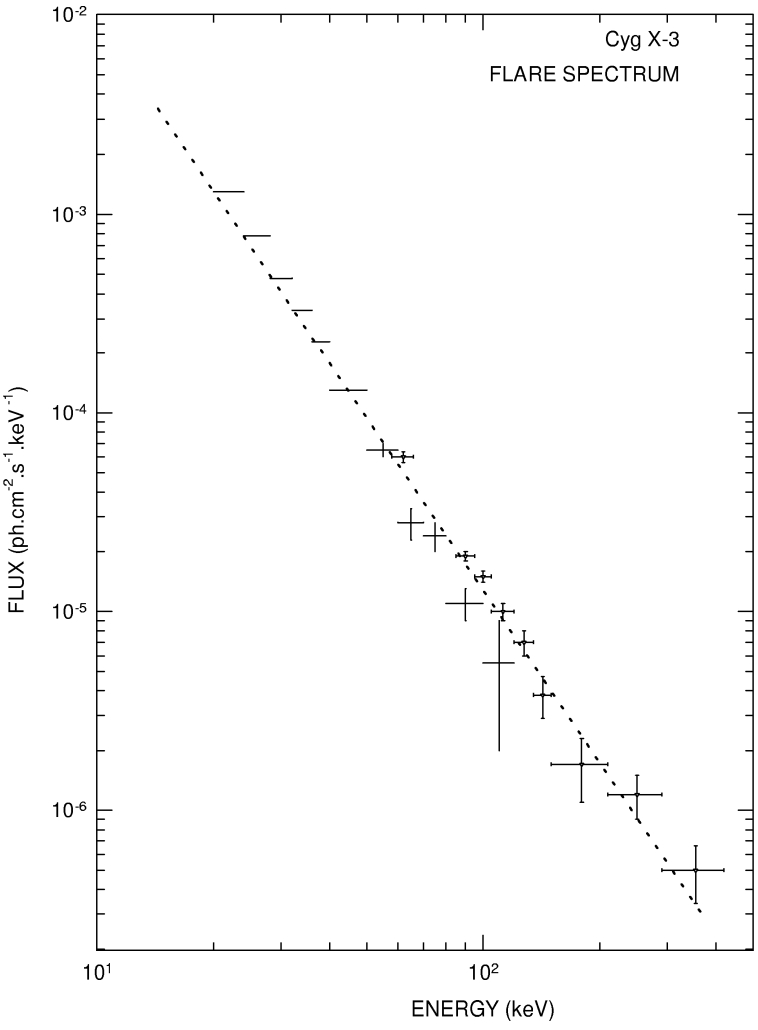

Figure 4. Hard X-ray spectrum of Cyg X-3 during flare period.

The prime factors which determine the X-ray emission mechanism and the accretion geometry of the source do depend to some extent on the nature of the compact object. In the case of a black hole or a low magnetic field neutron star, the X-ray emission is believed to arise in the inner edges of the accretion disk. In the case of a neutron star with strong magnetic field, the photon emission from the hot spot at the polar cap is considered as the most probable cause. The source luminosity and its temporal behaviour at macroscopic scale is a direct result of the variation in the accretion rate. In the standard model for accretion in binary system the transfer of the mass from the primary to the compact object takes place either through the Roche lobe overflow or by the stellar wind. Since the accreting gas will have intrinsic angular momentum, a Keplarian disk will be formed around the compact object and the falling matter releases the gravitation potential energy, which heats the gas and emits radiation. The exact spectral behaviour of the emergent photons will be determined by the accretion geometry, dominant heating and cooling mechanism, optical thickness of the gas in

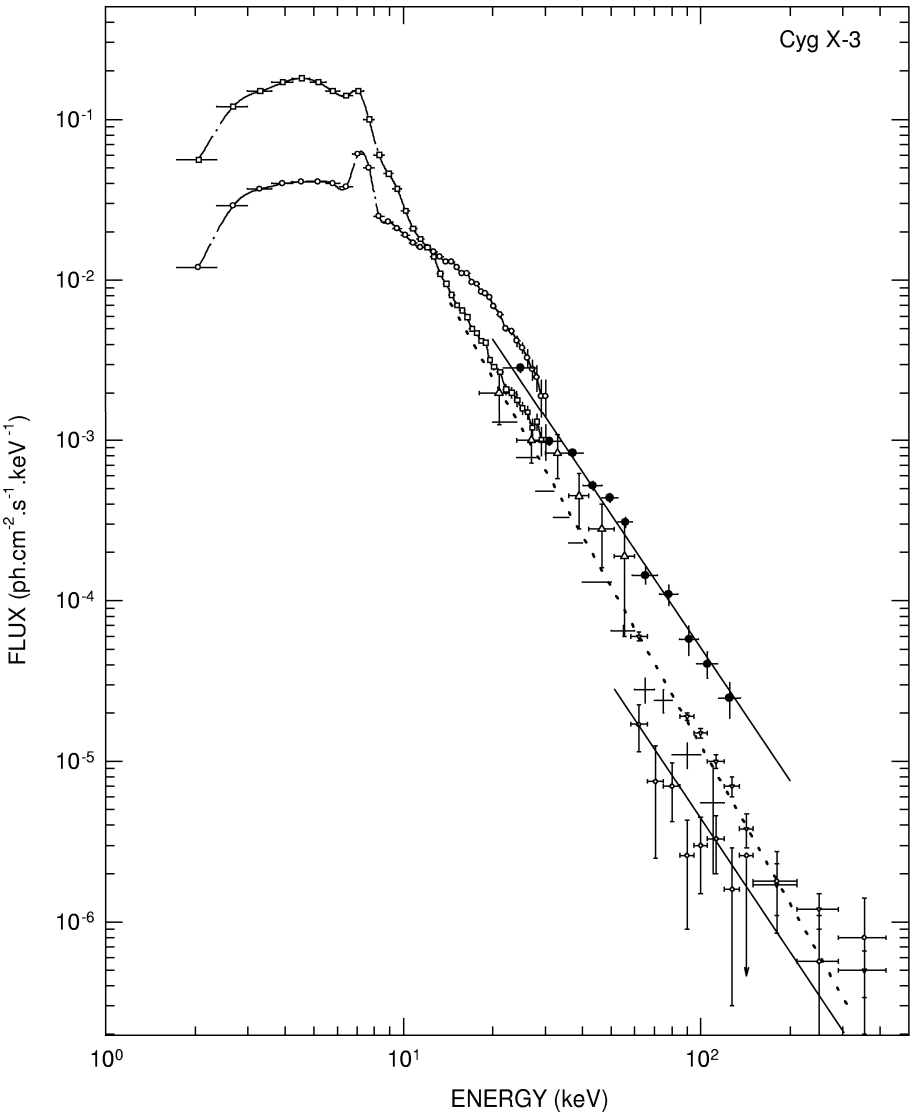

Figure 5. A compilation of the spectral data of Cyg X-3 in the 2–500 keV range. ○ Nakamura *et al.*, Δ Rao *et al.*, − − − HEXE, + OSSE, • Present data. Solid lines represent the best fit power law band corresponding to the different activity levels in quiescent phase.

the emission region, net heating and cooling rates, radiation pressure, magnetic fields and the boundary conditions at large distance as well as stellar surface. (Shapiro & Teukolsky 1983; King 1997). Thus a unified model leading to the emergent spectrum will reflect the dominance of one or more processes in the emission geometry. In the specific case of accretion on to a black hole compact object, the ultrasoft and the soft X-ray excess in the 2–10 keV energy region is expected due to the fact that the main cooling mechanism near to the surface of black hole is almost 100% advection (Chen *et al.* 1997; Narayan & Yi 1994, 1995a, 1995b) and the electron temperature does not rise to very high kT value.

While the long term X-ray variability of the source depends on the rate of accretion coupled to dynamical nature of the companion, the spectral and other temporal features need to be understood in terms of the standard model of accreting neutron star. In the case of Cyg X-3, the model parameters in the low energy region are derived by fitting the observed spectra with a large number of parameters with or without any physical connection to the natural changes expected during the change in the source activity. For example, in their attempt to make a unified fit to 2–30 keV data Nakamura *et al.* (1993) use a 13 parameter fit. The components include, a free-free emission spectrum, a black body spectrum, iron emission line and an ad hoc absorption edge at 9 keV and a variable absorbing medium for the line and continuum. To explain the hard X-ray measurements presented in section 2, it is essential to include further assumptions in these unified models. Even though some of the global features are clearly seen in the composite data shown in Fig. 5, the ensemble of a large number of parameters is too artificial. A simple composite model based on the global properties of the source will provide a natural geometry for the emission region. The observed global features as seen in various figures are summarized in Table 1.

Table 1. Summary of the observed spectral parameters of Cyg X-3.

	High state	Low state
α_1 in hard X-rays	3.25 ± 0.1	2.3 ± 0.1
E_{Fe} [keV]	6.53 ± 0.03	6.53 ± 0.02
EW_{Fe} [keV]	1.1	2
Estimated Compton scattered contribution (1–50 keV) 10^{-9} ergs cm^{-2}s^{-1}	3.8	4.4

We propose that the seed photons and the low energy continuum spectrum of Cyg X-3 is produced in a free-free emission process (Becket *et al.* 1978; Blisset *et al.* 1981) in the 2–500 keV band and the resultant spectrum is further modified by the Comptonization of the low energy photons (Sunyaev & Titarchuck 1980). In a hot tenuous plasma bremsstrahlung and recombination losses are small and the energy exchange between electrons and photons is controlled by the multiple scattering. For $4kT_e > h\nu$, the seed photons are upgraded in energy and a composite power law spectrum emerges due to the superposition of the photons scattered by differing number of times. The spectral index will thus be determined by the average number of scattering per photon. In a non-relativistic plasma where $kT_e \ll m_e c^2$ and $\tau \gg 1$, the average number of scattering for the seed photon $n_s \sim \tau^2$. Clearly the optical depth of the scattering envelope will control the hard X-ray spectrum. We have plotted sample simulated spectra obtained through Comptonization of the low energy photons in weakly relativistic plasma in Fig 6. The curves correspond to two optical depths of $\tau \sim 0.1$ and $\tau \sim 1$ are computed using Monte-Carlo method (Pozdnyakov *et al.* 1983).

It is seen from the figure that an increase in the optical depth of the plasma cloud leads to flattening of the emergent spectrum as well as deficit in the low energy band. The curves are normalized to the observed of Cyg X-3 at 10 keV. Therefore, the observed power law nature of the hard X-ray spectrum and reduction in the low energy photons during the low/hard state of Cyg X-3 can thus be accounted as due to the enlargement of

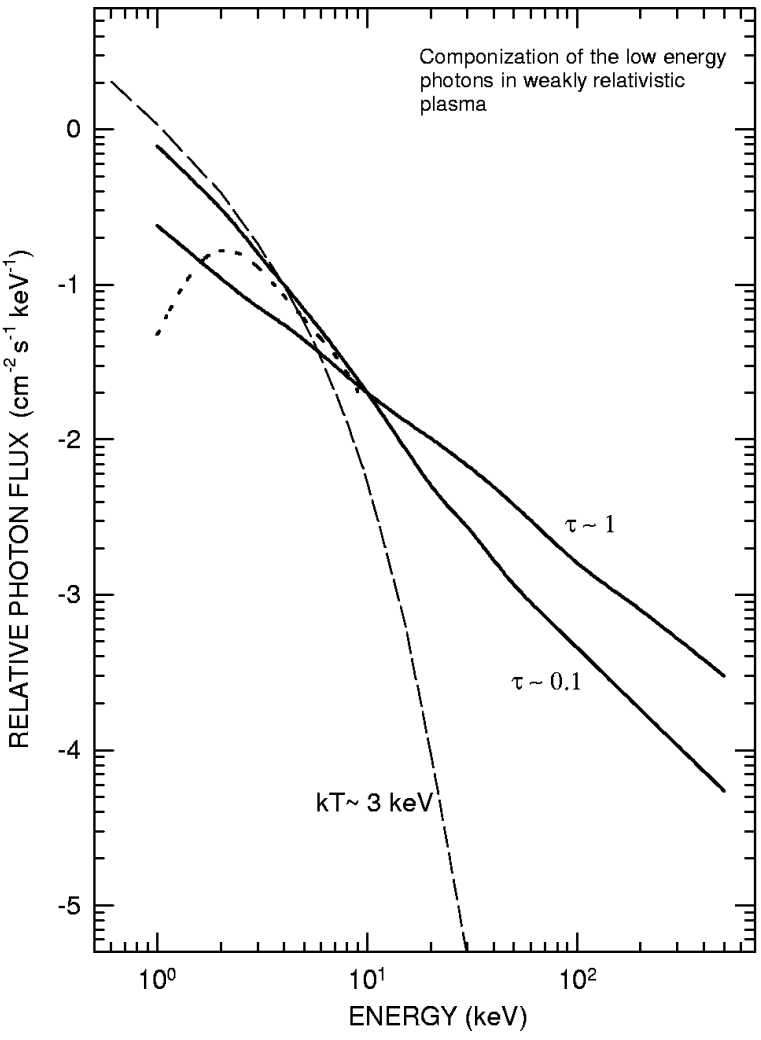

Figure 6. Sample curves for Comptonized low energy photons in a cloud of weekly relativistic plasma for two values of optical depths and differing number of scattering.

the surrounding cloud of relativistic plasma. A lower mean energy of the iron emission line at 6.53 ± 0.02 keV also supports the presence of the hot plasma cloud. In such a model, the flux of 6.5 keV iron emission line will also be proportional to the optical depth of the scattering cloud and the line energy will be independent of the intensity state of the source. Therefore, during the low/hard state, the larger optical depth will lead to the increased equivalent width of the line. The observed data shown in table 1, clearly supports this hypothesis.

In Fig. 6, we have also plotted a free-free emission spectrum with kT $\approx$ 3 keV. The data are normalized at 6 keV. It is seen from the figure that apart from the contribution arising from the iron emission line, a thermal emission from a hot plasma does represent the general spectral behaviour of the source in the low energy band and could provide the necessary seed photons for Comptonization. A non-exponential, gradual

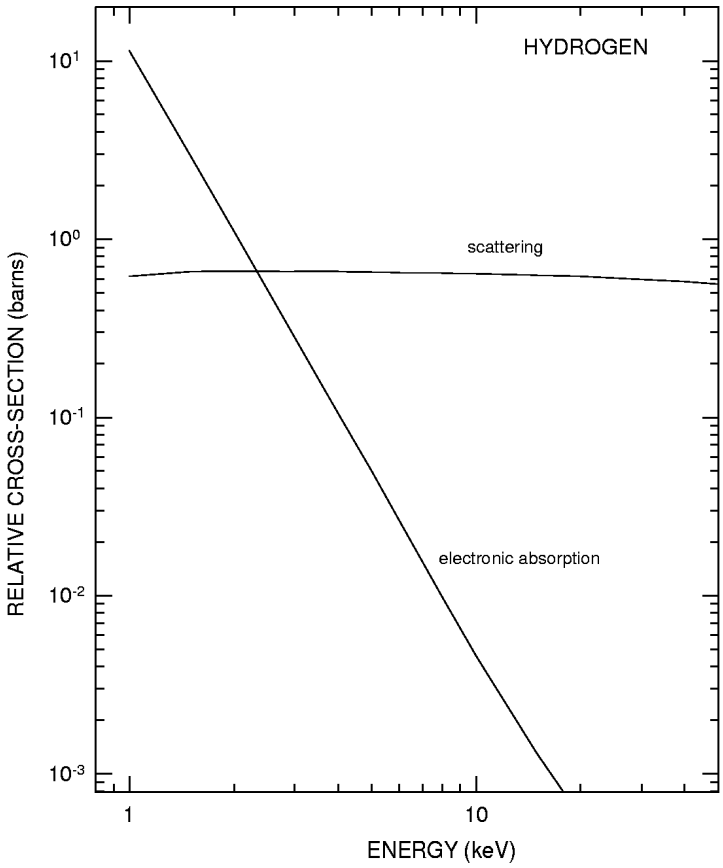

Figure 7. Attenuation cross section vs. photon energy for hydrogen.

turn-around in the observed spectrum below 5 keV as seen in figure 5, can be easily reproduced by a cold hydrogenous shell. The presence of a cold matter around the source is clearly indicated by the asymmetry of the light curve both in the X-ray and infrared bands (Kitamoto *et al.* 1994b). In the case of hydrogen, the electronic absorption cross section for photons is only dominant below 3 keV as shown in Fig. 7. Above 3 keV, photon interactions only lead to degrading the photon energy as opposite to total loss. The shape of resultant spectrum is thus radically modified due to multiple Compton scattering compared to the simple exponential attenuation (Manchanda 1976). In Fig. 6, the dotted line shows the expected low energy behaviour of the spectrum including the build-up effect due to multiple Compton scattering in a cold shell of thickness 0.5 gm.cm^{-2}(3×10^{26}). It is clearly seen from Fig. 6 that computed curves account for the global features in the observed X-ray spectrum of source as seen in Fig. 5.

Two important questions which need to be addressed in support of the proposed model are, the origin and maintenance of the hot plasma cloud surrounding the hot spot and the presence of the cold matter in the line of sight. The two mechanisms which easily give rise to the hot plasma cloud are the X-ray driven wind or the winds driven by the poloidal magnetic field. The dynamics of Compton heated winds and coronae that may form above an accretion disk irradiated by an intense X-ray flux at critical

and super critical luminosities have been discussed in the literature (Begelman *et al.* 1983; and Jones & Raine 1980). Evidence of an X-ray driven wind was seen in strong optical emission with weak P Cyg profiles early in the outburst of V404 Cygni (Wagner *et al.* 1991). Optically thin thermal bremsstrahlung in the X-ray driven hot wind at $\sim 10^6$ K has been proposed to explain the infrared excess observed from the black-hole transient A0620-00. Similarly the correlated H_α excess to the X-ray luminosity of GX 1 + 4 has been explained by the reprocessing of the EUV flux generated from the free-free emission in the wind (Manchanda *et al.* 1995). The observed X-ray luminosity $L_x \approx 10^{37} - 10^{38}$ erg s^{-1} of Cyg X-3 corresponds to a mass accretion rate $\dot{M} \sim 10^{17} - 10^{18}$ g s^{-1}. The radius and temperature of the outer region of the accretion disk formed by this accreted matter are respectively given by

$$R_{\rm disk} > 3.2 \times 10^3 \dot{M}_{17}^{\frac{2}{3}} r_s \quad \text{and} \quad T_s \sim 2 \times 10^7 \dot{M}_{17}^{\frac{1}{4}} \left(\frac{r}{r_s}\right)^{-\frac{3}{4}}$$

for a neutron of mass $1.4\,M_\odot$ and radius $r_s \sim 10^6$ cm (Shapiro & Teukolsky 1983). For a value of $R_{\rm disk} \sim 10^{10} - 10^{11}$ cm, the outer layer should radiate at a black body temperature of $T \leq 10^4 - 10^5$ K. The total emissivity due to the wind can be written as;

$$4\pi \int_0^\infty J_\nu d\nu = 1.435 \times 10^{-27} T^{1/2} n_e^2 \text{ erg cm}^{-3}\,\text{s}^{-1}.$$

For a temperature $T \sim 10^5$ K the total contribution from the wind is estimated to be $\leq 2 \times 10^{35}$ erg s^{-1} for $n_e^2 V \sim 10^{60}$. Thus the X-ray driven winds can sustain the hot plasma necessary for Compton upgrading of the low energy X-ray photons.

An alternate mechanism which can drive the hot plasma is the wind caused by centrifugal motion of the magnetized plasma in the disk. Presence of transient radio jets for Cyg X-3 have been discussed in literature (Manchanda *et al.* 1993; Mirabel & Rodriguez 1994; Miduszewski *et al.* 1998, 2001). A magneto-centrifugal wind has been discussed as the underlying mechanism for the spurting jets in which the ionized particles within the accretion disk are out along magnetic field lines that ultimately twist into a helical shape along the rotational axes of the disk. Orbital energy from the accretion disk is thus dissipated in propelling the polar jets (Königl A. 1989). Detailed models for the origin of the MHD wind and its collimation into a jet from the surface of Keplarian accretion disks have been discussed in literature (Pelletier & Pudritz 1992; King & Kolb 1999). A geometrical model involving magnetocentrifugal wind is consistent with the episodes of jet ejection observed in Cyg X-3 (Miduszewski *et al.* 1998). The steady state angular momentum equation of an axisymmetric accretion disk threaded by the magnetic field and undergoing viscous stress depends upon the angular momentum of the accreting matter $\rho u_p \Omega r^2$, the ordered magnetic energy density in the disk $\frac{r B_\phi B_p}{4\pi}$ and the viscous torque $\tau_{\rm visc}$. For a dipole field, the B_ϕ is taken as B_z. We propose that poloidal magnetic field in the accretion disk grows on arbitrary time scale depending upon the accretion rate and the development of instabilities in the disk and when sufficiently strong, this component can then drive the magneto-centrifugal wind and even the ejection of a jet. It has been shown that poloidal magnetic flux may be dragged radially inward by the accreting gas until its dissipative escape, driven by the gradient in magnetic pressure limits its growth. Provided that the magnetic field makes an angle of less than 60° with the radius vector at the disk in Keplarian motion,

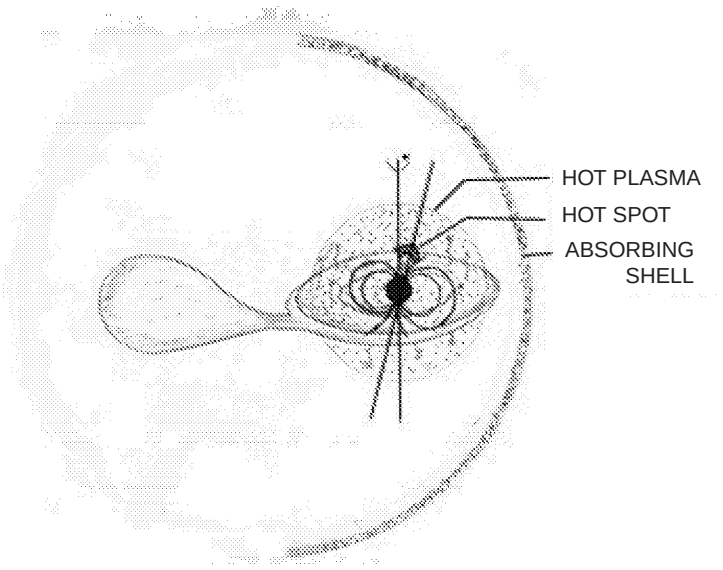

Figure 8. A schematic diagram of the geometrical model.

it will be energetically favorable for gas to leave the disk in a centrifugally driven wind (Blandford 1989; Königl & Ruden 1992).

The origin of the large amount of cold material made of mostly hydrogenous matter in the line sight may be connected with the Wolf-Rayet nature of the companion star. High velocity strong winds are the observed characteristics of WR stars. It is therefore, conceivable that outside the capture radius in a wind-fed geometry, a cold shell may be formed at the interaction boundary of the wind and the primordial hydrogenous material swept by the WR wind.

In summary, a simple thermal source embedded in a relativistic plasma within a cold shell can easily reproduce the observed spectral features of Cyg X-3. The spectral index and the intensity of the iron emission line being dependent on the optical depth of the relativistic cloud. We have made no attempt to derive the set parameters which can fit the observed data shown in Fig. 5 as the observations were made at very different epochs. The absence of the coherent pulsation and the assumption of the neutron star with strong magnetic field giving polar emission considered in our model do not pose any problem. A cartoon picture depicting emission geometry in Cyg X-3 is shown in Fig. 8. It is seen from the figure that in a general case, the value of viewing angle θ, angle of the emission cone α and the angle between the rotation and magnetic axis of the compact object β do control the observance of any pulsation or its shape. The absence of pulsation and the binary modulation in the radio jet in Cyg X-3 suggests that the viewing angle must be $< \beta$ with respect to the rotation axis.

Acknowledgements

I thank Sarvashri J. A. R. D'Silva, P. P. Madhwani, N. V. Bhagat, B. G. Bagade and Ms. N. Kamble for their support in the fabrication of the payload and flight support. I also thank the staff at the TIFR balloon facility, Hyderabad for fabricating the balloon

and conducting a successful balloon flight. I also gratefully acknowledge the RXTE and BATSE teams for making their data public on their respective web sites.

References

Becker, R. H., Robinson-Saba, J. L., Boldt, E. A., Holt, S. S., Pravado, S. H., Serlimitsos, P. J., Swank, J. H. 1978, *Ap.J.*, **224**, L113.
Blisset, R. J., Mason, K. J., Culhane, J. L. 1981, *MNRAS*, **194**, 77.
Begelman, M. C., McKee, C. F., Shields, G. A. 1983, *Ap.J.*, **271**, 70.
Bhat, P. N., Ramana Murthy, P. V., Vishwanath, P. R. 1988, *JApA*, **9**, 155.
Blandford, R. D. 1989, In: *Theory of Accretion Disks*, (ed.) P. Meyer, W. Duschl, J. Frank and E. Meyer-Hofmeister (Dordrecht: Kluwer), 35.
Bonnet-Bidaud, J. M., Chardin, G. 1988, *Phys. Rep.*, **170**, 326.
Chadwick, P. M., Dipper, N. A., Dowthwaite, J. C., Gibson, A. I., Harrison, A. B. 1985, *Nature*, **318**, 642.
Chardin, G., Gerbier, G. 1989, *A& A*, **210**, 52.
Chen, X., Abramowicz, M. A., Lasota, J. 1997, *Ap.J.*, **485**, L75.
Chitnis, V. R., Agrawal, P. C., Manchanda, R. K., Rao, A. R. 1993, *BASI*, **21**, 555.
D'Silva, J. A. R., Madhwani, P. P., Tembhurne, N., Manchanda, R. K. 1998, *NIM*, **A412**, 342.
Dal Fiume, D., Palazzi, E., Orlandini, M., Nicastro, L., Del Sordo, S. 2000, *IAUC*, **7393**.
Ergam, E., Youngelson, Lev R. 1998, *A& A*, **333**, 151.
Jones, B. C., Raine, D. J. 1980, *A& A* **81**, 128.
Kitamoto, S., Kawashima, K., Negoro, H., Miyamoto, S., White, N. E., Nagase, F., 1994a, *PASJ*, **46**, L105.
Kitamoto, S., Mizobuchi, S., Yamashita, K., Nakamura, H. 1992, *Ap.J.*, **384**, 263.
Kitamoto, S., Miyamoto, S., Waltman, E. B., Fiedler, R. L., Johnston, K. J., Ghigo, F. D. 1994b, *A& A*, **281**, 85.
Kafuko, S., Yamaguchi, S., Yamaguchi, M., Kawai, N., Matsuoka, M., Koyama, K., Kifune, T. 1994, *MNRAS*, **268**, 437.
King, A. 1997, In: *Accretion Disks - New Aspects*, (Springer-Verlag.) p 356.
King, A. R., Kolb, U. 1999, *MNRAS*, **305**, 654.
Königl, A. 1989, *Ap.J.*, **342**, 208.
Königl, A., Ruden, S. P. 1992, In: *Protostars and Planets III*, (eds) E. H. Levy, & J. I. Lunine, (University of Arizona Press).
Liang, E. P., Nolan, P. L. 1984, *Space Sci. Rev.*, **38**, 353.
Manchanda, R. K. 1976, *IJRSP*, **5**, 13.
Manchanda, R. K. 1998, *Adv. Sp. Res.*, **21**, 1019.
Manchanda, R. K., Waldron, L., Sood, R. K. 1993, *PASAu*, **10**, 208.
Manchanda, R. K., Lawson, W. A., Grey, D. J., Sood, R. K., Sharma, D. P., James S. 1995, *A& A*, **293**, 29.
Mirabel, I. F., Rodriguez, L. F. 1994, *Nature*, **375**, 464.
Mori, M., Bertsch, D. L., Dingus, B. L., Esposito, J. A. *et al.* 1997, *Ap.J.*, **476**, 842.
Matz, S. M., Garabelsky, D. A., Purcell, W. R., Ulmer, *et al. AIP Conference Proceedings* (ed.) S. Holt & S. D. Charles, 1994, **308**, p. 263
Matz, S. M., Fender, R. P., Bell Burnell, S. J., Groove, J. E., Strickman, M. S. 1996, *A& A Suppl.* **120**, 235.
Maisack, M., Kendziorra, E., Pan, H., Skinner, G., Englhauser, J., Reppin, C., Efremov, V., Sunyaev, R. 1994, *Ap J Suppl*, **92**, 473.
Miduszewski, A. J. *et al.* 1998, In: *ASP Conf* (eds.) J. A. Zeusus, G. B. Taylor & J. M. Wrobel, **144**.
Miduszewski, A. J., Rupen, M. P., Hjellming, R. M., Pooley, G. G., Waltman, E. B. 2001, *Ap.J.*, **533**, 766.
Newell, S. J., Garrett, M. A., Spencer, R. E. 1998, *MNRAS*, **293**, L17.
Nakamura, H., Matsuoka, M., Kawai, N., Yosihada, A., Miyoshi, S., Kitamoto, S., Yamashita, K. 1993, *MNRAS*, **261**, 353.
Narayan, R., Yi I. 1994, *Ap.J.*, **428**, L13.

Narayan, R., Yi I. 1995a, *Ap.J.*, **444**, 213.
Narayan, R., Yi I. 1995b, *Ap.J.*, **452**, 710.
Ogley, R. N., Bell Burnell, S. J., Spencer, R. E., Newell, S. J. *et al.*, 2001, *MNRAS*, **326**, 349.
Paerels, F., Cottman, J., Sako, M., Liedahl, D. A. *et al.*, 2000, *Ap.J.*, **533**, L135.
Pelletier, G., Pudritz, R. E. 1992, *Ap.J.*, **394**, 117.
Pozdnyakov, L. A., Sobol, I. M., Sunyaev, R. A. 1983, *Space Sci. Rev.*, **2**, 189.
Predehl, P., Burtwitz, V., Paerels, F., Trumper, J. 2000, *A& A*, **357**, L25.
Rajeev, M. R., Chitnis, V. R., Rao, A. R., Singh, K. P. 1994, *Ap.J.*, **424**, 376.
Rannot, R. C., Bhat, C. L., Tickoo, A. K., Sapru, M. L., Senecha, V. K., Kaul, V. K. 1994, *Ap& SS*, **219**, 221.
Rao, A. R., Agrawal, P. C., Manchanda, 1991, *A& A*, **241**, 127.
Schmutz, W, Gebelle, T. R., Schild, H. 1996, *A& A*, **311**, L25.
Shapiro, S. L., Teukolsky, S. A. 1983, In: *Black holes, White dwarfs & Neutron stars*, (John Wiley & Sons).
Sunyaev, R. A., Titarchuk, L. G. 1980, *A& A*, **86**, 121.
van Kerkwijk, M. H., Charles, P. A., Gebelle, T. R. *et al.* 1992, *Nature*, **355**, 703.
Van Kerkwijk, M. H. 1993, *A& A*, **276**, L9.
Van Kerkwijk, M. H., Gebelle, T. R., King, D. L., van der Klis, van Paradijs, 1996, *A& A*, **314**, 521.
van der Klis, M., Jensen, F. A. 1985, *Nature*, **313**, 768.
Wagner, R. M., Bertram, R., Starrfield, Sumner G., Howell, Steve B., Kreidl, Tobias J., Bus, S. J., Cassatella, A., Fried, R., 1991, *Ap.J.*, **378**, 293.
White, N. E., Holt, S. S. 1982, *Ap.J.*, **257**, 318.
White, N. E., Nagase, F., Parmar, A. N. 1992, In: *X-ray Binaries*, (ed.) Lewin, Paradijs & van den Heuvel (Cambridge. Univ. Press), 1.
Willingale, R., King, A. R., Pounds, K. A. 1985, *MNRAS*, **215**, 295.